SHAKE-TABLE TESTING OF HYBRID POST-TENSIONED PRECAST WALL SYSTEMS WITH ALTERNATIVE DISSIPATING SOLUTIONS

D.J. Marriott[1], S. Pampanin[2], A. Palermo[3], D. Bull[4]

[1] *Ph.D. Candidate, Dept. of Civil and Natural Resources Engineering, University of Canterbury. New Zealand*
[2] *Senior Lecturer, Dept. of Civil and Natural Resources Engineering, University of Canterbury. New Zealand*
[3] *Assistant Professor, Dept. of Structural Engineering, Politecnico di Milano, Milan.Italy*
[4] *Adjunct Professor, Dept. of Civil and Natural Resources Engineering, University of Canterbury. New Zealand*

ABSTRACT :
It is fast becoming common practice for civil engineering infrastructure and building structures to be designed to achieve a set of performance objectives. To do so, consideration is now being given to systems capable of sustaining minimal damage after an earthquake while still being cost competitive. This has led to the development of high performance seismic resisting systems, followed by advances in design methodologies.
The paper presents the experimental response of four pre-cast, post-tensioned rocking walls with high-performing dissipating solutions tested on the shake-table at the University of Canterbury. The wall systems were designed as a retrofit solution for an existing frame building however, can also be used for the design of new, high-performance structures. The use of externally mounted dampers allowed numerous dissipation schemes to be explored including mild-steel dampers (hysteretic dampers), viscous dampers, a combination of both or no dampers. The advantages of both velocity and displacement dependant dissipation was investigated for protection against strong ground motions with differing rupture characteristics i.e. far-field and near-field events.
The experimental results are used to verify a proposed design procedure for post-tensioned rocking systems with supplementary hysteretic and viscous dissipation. The predicted response compared well with the measured shake-table response.

KEYWORDS: Post-tensioning, dissipation, shake-table, high performance

1. INTRODUCTION

The structural performance of precast structures with unbonded post-tensioning can surpass equivalently reinforced monolithic counterparts with respect to building structures (Priestley [1999], Kurama [2002], Pampanin [2005], Solberg et al. [2008]) and bridge systems (Kwan and Billington [2003] and Palermo et al. [2005]). This enhanced performance is due to inelastic deformation being lumped to a discrete number of specifically designed and detailed rocking interfaces. An example is illustrated in Figure 1 (a) and (b) where a post-tensioned, pre-cast rocking wall is installed with replaceable externally mounted mild steel dampers. In this example, the dampers are designed to yield in tension and compression and are restrained against buckling. This type of damper is termed a TCY hysteretic damper (tension-compression-yielding). As the wall displaces laterally an opening occurs at the rocking interface (Figure 1 (b)) elongating the dampers and the post-tensioned tendons. The ratio of the prestressed reinforcement (and axial load) to the non-prestressed reinforcement defines the energy dissipation and re-centring properties of the wall system – these two parameters give an indication of the expected maximum displacement and residual deformation of the system following dynamic response. This technology has been codified in the U.S. (ACI:T1.2-03 [2007]) and in New Zealand (NZS3101 [2006]) and is termed “Hybrid or Controlled Rocking” Technology. In this contribution a design procedure for post-tensioned rocking systems with supplementary dissipation is presented and supported with experimental shake-table testing. The results from a series of free vibration release tests are presented to quantify the contact damping associated with impact at the rocking interface. In particular, the free vibration response of two precast wall units is discussed; one having no supplementary dissipation and the other with a low level of hysteretic damping. Following from this, the shake-table was used to subject three precast walls to a strong ground motion. The input motion was scaled to a design acceleration spectrum representing a probability of excedance of 2% in 50 years i.e. a maximum considered event (MCE). The maximum displacement response is compared with the predicted displacement following the proposed design procedure.

2. DESIGN OF POST-TENSIONED WALLS WITH SUPPLEMENTARY DISSIPATION

Hybrid structures are inherently high performing and are generally associated with low damage. These systems

may in fact achieve much higher levels of performance when considering residual deformations, repair and downtime. A general load deflection response is shown in Figure 1 (c) with significant damage only occurring when excessive compression strains cause failure of the toe region, or rupture of the mild-steel or prestressed reinforcement occurs. Recommendations from Kurama et al. [1999], fib [2003], Priestley et al. [2007] have been used to define three performance objectives for post-tensioned wall systems: Immediate occupancy, damage control or life safety and collapse prevention. These performance objectives are discussed in further detail in Marriott et al. [2008] along with performance objectives related to the retrofit of existing structures with supplementary post-tensioned rocking walls.

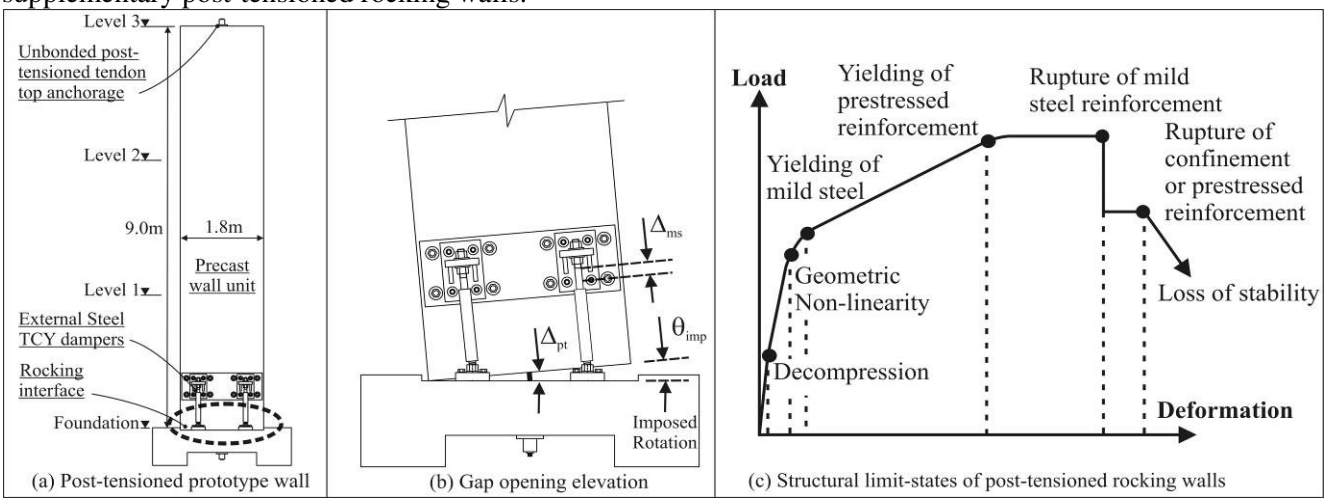

Figure 1 Post-tensioned precast rocking wall system with externally mounted mild steel dampers

Research has shown that post-tensioned rocking systems, in particular, are ideally suited to a Direct Displacement-Based Design (DDBD) framework (Priestley [2003] and Palermo et al. [2005]). With this in mind, a DDBD procedure is proposed for post-tensioned wall systems incorporating supplementary viscous and hysteretic dissipation devices (Figure 2).

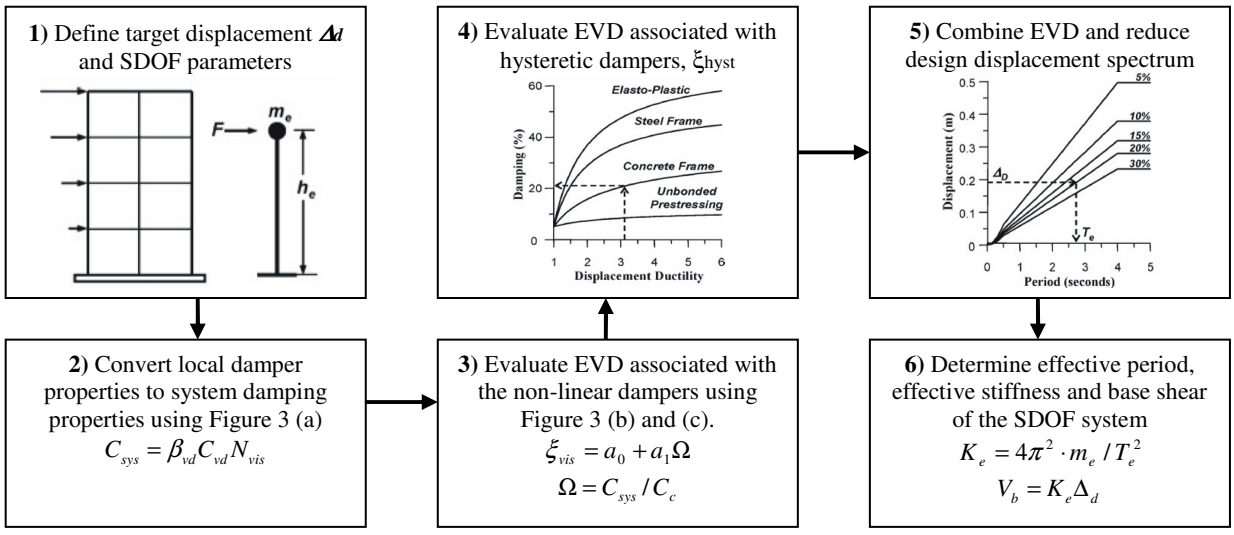

Figure 2: Design of post-tensioned walls with supplementary dissipation (adapted from Priestley et al. [2007])

The procedure builds upon traditional DDBD (Priestley et al. [2007]), equating the equivalent viscous damping (EVD) associated with the supplementary non-linear viscous dampers located at the rocking interface.
While a summary of the design procedure is outlined here, a complete design example is presented in the appendix of the paper with more details.
Step 1: The SDOF parameters are defined i.e. the displacement Δ_d of the effective mass m_e at the effective height h_e.
Step 2: The local damper coefficient C_{vd} is converted to a global damping coefficient C_{sys} using Figure 3 (a) which is

based on the aspect ratio A_r of the section and the non-linearity of the damper α.

Step 3: The system damping C_{sys} is normalised with respect to critical damping C_c of the system defining Ω. The EVD ξ_{vis} is determined using Figure 3 (b) for far-field seismicity or (c) for near-field seismicity.

Step 4: The hysteretic EVD ξ_{hyst} is calculated based on the system ductility μ and the moment ratio between the mild-steel reinforcement and the prestressed reinforcement λ.

Step 5: The total system EVD is computed and the design displacement spectrum is reduced by the damping reduction factor η, which then defines the effective period T_{eq}.

Step 6: The secant stiffness K_{eq} multiplied by the displacement Δ_d of the SDOF system defines the base shear V_b.

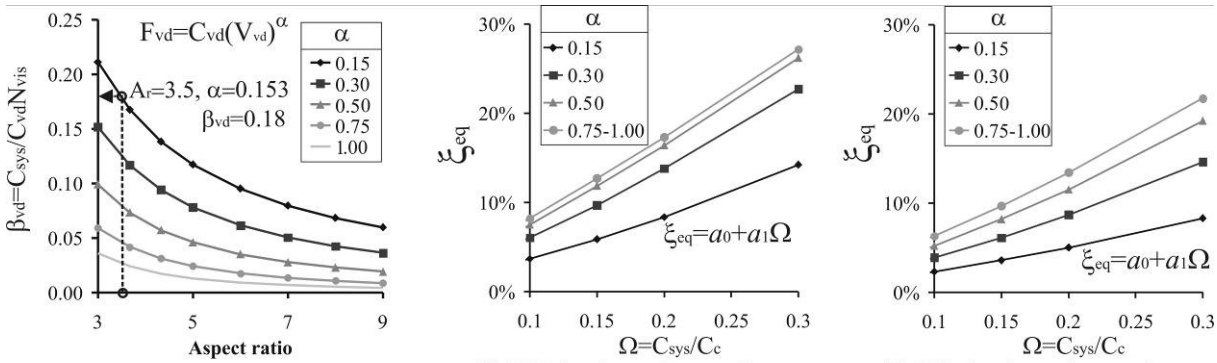

(a) Ratio of local to global damping coefficients

(b) EVD for viscous dampers for *far-field* strong ground motion

(C) EVD for viscous dampers for *near-field* strong ground motion

Figure 3 System damping coefficient and equivalent viscous damping (EVD) relationships

3. EXPERIMENTAL PROGRAMME

An experimental programme was undertaken at the University of Canterbury to investigate both the cyclic and dynamic performance of 1/3 scale post-tensioned rocking wall systems with alternative energy dissipating mechanisms. The experimental programme was divided in two phases. The first phase investigated the response of post-tensioned walls subjected to high speed sinusoidal loading at increasing levels of amplitude and frequency from 0.1Hz through to 2.0Hz. In the second phase the dynamic response was examined from free vibration testing and earthquake excitation. For brevity, the free vibration response of two walls is discussed, followed by dynamic testing of three walls subjected to a strong ground motion.

The shake-table test set-up is illustrated in Figure 4. A 3840kg pendulum mass was suspended by the laboratory crane. This set-up proved very effective in providing a consistent driving mass. Out-of-plane restraint of the wall was provided by steel channels with frictionless rollers located between the wall and steel channels.

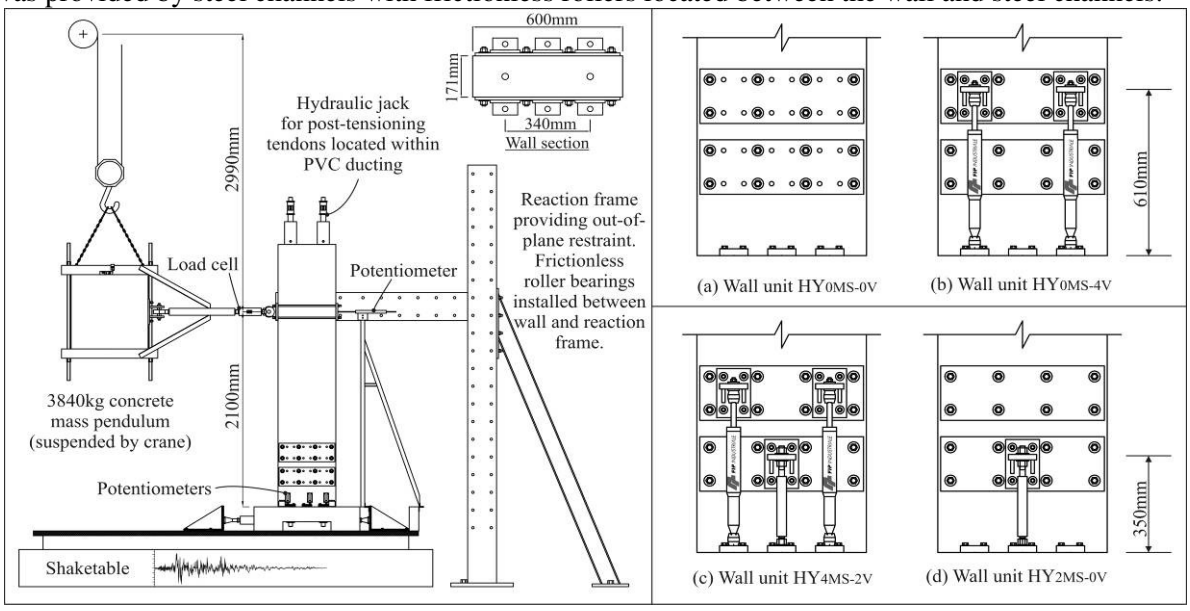

Figure 4 Shake-table set up (left) and precast wall specimens (right (a)-(d))

The nomenclature used to identify each post-tensioned wall is HY**x**MS-**y**V where ***x*** is the number of TCY hysteretic dampers, and ***y*** is the number of viscous dampers located at the rocking interface (refer Table 1).

Table 1 Details of the dissipation mechanisms and post-tensioning of the four precast walls

Wall	Post-tensioning details	Damper device details
HY0MS-0V	2 tendons each stressed to 50kN (0.323f_{pty})	-
HY0MS-4V	2 tendons each stressed to 30kN (0.194f_{pty})	4 viscous dampers (courtesy of *FIP Industriale*)
HY4MS-2V	2 tendons each stressed to 20kN (0.130f_{pty})	4 viscous dampers plus 2 TCY mild steel dampers
HY2MS-0V	2 tendons each stressed to 40kN (0.259f_{pty})	2 TCY mild steel dampers

3.1 Construction details of the post-tensioned precast wall units

Construction details of the walls were typical of precast construction with the inclusion of two PVC ducts running the height of the wall to locate the unbonded post-tensioned tendons. A fabricated steel angle was cast within the base of the wall for confinement of the toe region (Figure 5(b) and (c)). A recess was also cast into the top of the foundation to locate the precast wall when lowered into position. When the wall corrected located a high flow epoxy grout (Sikadur 42) was pumped under pressure around the recess and beneath the rocking interface. This provided ample shear transfer and prevented slip along the rocking interface. A cavity was located on the underside of the foundation to allow access to the tendon anchorages.

The external dissipation devices were connected to the wall by stiff steel brackets Figure 5(b). These steel dissipater brackets were bolted to a steel plate which was fixed rigidly to side of the precast concrete wall Figure 5(c). Two steel plates were fixed to each side of the wall to accommodate a maximum of 3 dampers per side with two length options.

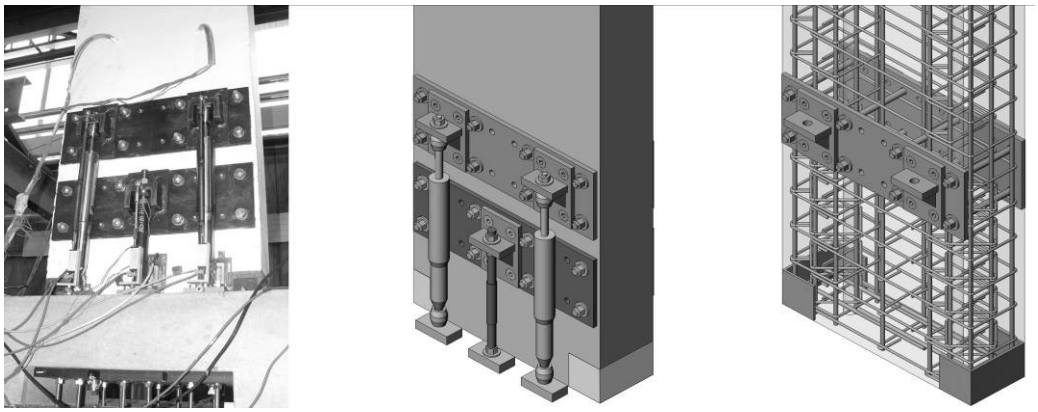

(a) As-built post-tensioned wall (b) Connection detail (c) Reinforcement, confinement and steel bracket details

Figure 5 Post-tensioned, precast wall unit (*CAD images courtesy of T. Smith*)

3.2 Performance of the damper devices

The performance of the dissipaters were extensively tested and quantified prior to testing within the precast wall. Cyclic testing of the TCY hysteretic dampers is presented in Figure 6 (a). The response is extremely stable as compression buckling is prevented due to a steel tube located over the yielding region. The steel tube is injecting with an epoxy grout for adequate restraint. Sinusoidal frequency testing of the non-linear viscous dampers (devices courtesy of *FIP Industriale*) is presented Figure 6 (b). The viscous dampers have a velocity power coefficient of α=0.15, therefore having relatively limited dependency on velocity.

3.3 Selection of the earthquake records for dynamic testing

A total of six ground motions (two records at each of the three intensity levels) were applied to each post-tensioned wall: the results from one record is given here. Careful selection of the records was required due the limitation of the shake-table which restricted the input velocity to approximately 240mm/s. Considering similitude scaling (for a 1/3 scale model), the spectrum-scaled earthquake records could not exceed a velocity of 415mm/s without modifying the record. The records were scaled to the New Zealand uniform hazard spectrum NZS1170.5 [2004]. The ground motion

considered herein was recorded at Rio Dell Overpass, Cape Mendocino (Table 2).

Table 2. Earthquake record subjected to post-tensioned wall units

Earthquake record	Recording Station	Scaled PGA	Scaled PGV [mm/s]	Scale factor
Cape Mendocino	Rio Dell Overpass	0.382	434	0.992

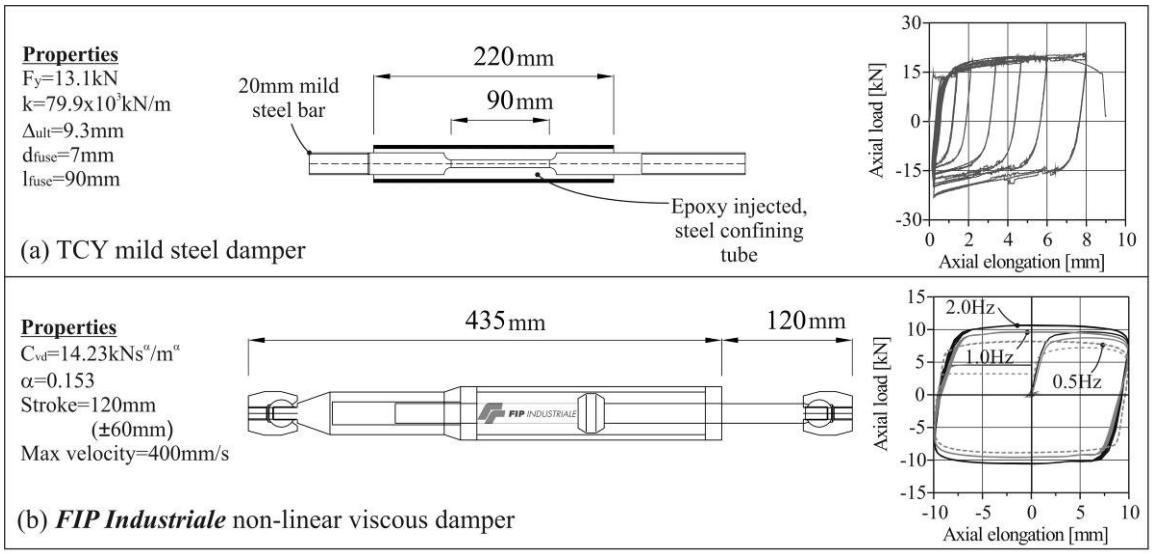

Figure 6. Supplementary damper properties

4. EXPERIMENTAL RESPONSE

4.1 Free vibration release testing

Three release amplitudes were chosen: 2.5%, 1.5% and 0.5% of lateral drift. The damped response (when released from an amplitude of 1.5% drift - 31.5mm) is shown for two precast wall units in Figure 7. The damping associated with rocking (referred to as contact damping) for the post-tensioned wall with no mechanical dampers ($HY_{0MS\text{-}0V}$) was then calibrated.

While a damping model proportional to the tangent stiffness proved to be more accurate, sufficient accuracy could be achieved with a constant damping formulation (refer Figure 7 (a)). The calibrated damping was found to be approximately independent of the release amplitude when a constant damping model was used based on the secant stiffness at release i.e. a constant damping equal to ***3.0%*** of critical damping, with critical damping formulated from the secant stiffness at release. This damping formulation has the advantage of being incorporated within a direct displacement-based design (DDBD) framework considering an elastic SDOF system with secant properties to the target displacement, Priestley et al. [2007]. While work is ongoing, the same proportion of damping appears appropriate for the post-tensioned wall with mechanical damping devices. This would suggest that the equivalent viscous damping associated with contact damping may be taken as a constant value of ***3.0%***, regardless of the target displacement, initial post-tensioning and supplementary dissipation.

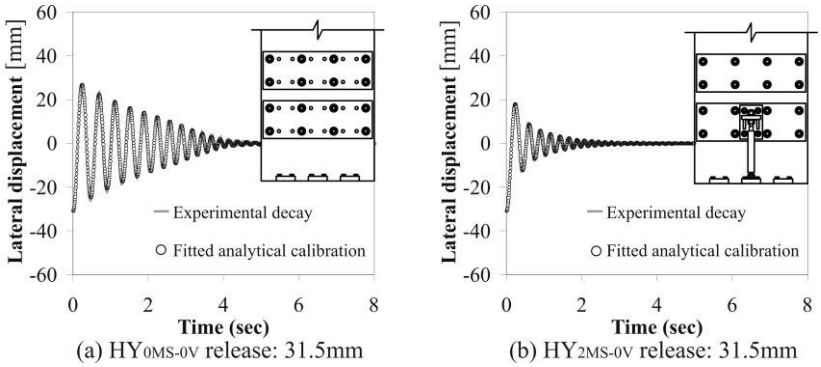

Figure 7: Free vibration release testing

4.2 Response to shake-table ground motion and performance evaluation

The measured response of the three prototype walls is presented in Figure 8, while the maximum displacement response is also compared with the predicted displacement response in Table 3. Of the three prototype walls, the system with viscous dampers alone (HY_{0MS-4V}) had the largest displacement response due the low EVD of the system. When combined with TCY dissipaters (HY_{2MS-4V}), the maximum displacement response was significantly reduced. The system with TCY dampers alone (HY_{2MS-0V}) returned the lowest maximum response. The magnitude of base shear is similar for all three walls – in fact each wall was designed to have a similar backbone but with varying energy dissipation.

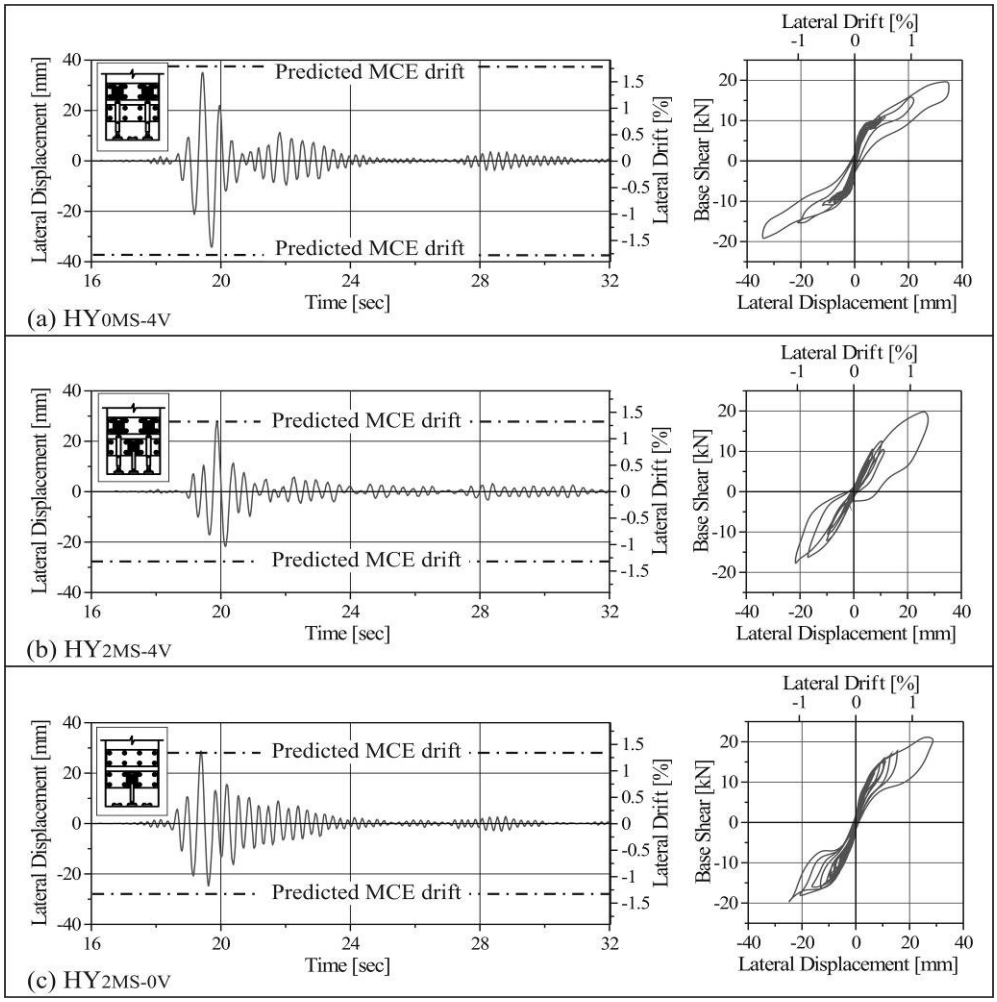

Figure 8. Experimental and predicted response of the three PT wall units under a MCE ground motion

The design objectives for the post-tensioned walls considered a drift ratio of 1.0% at the 2/3MCE level and a drift ratio of 1.5% at the MCE level, however because each post-tensioned wall had subtle differences in EVD, the maximum response of each prototype was expected to differ slightly. The proposed design procedure was used to assess/predict the displacement response of each wall (HY_{0MS-4V}, HY_{2MS-4V}, HY_{2MS-0V}) at the MCE hazard level. The predicted response is summarised in Table 3. The EVD in Table 3 is not an area-based damping; it is the EVD used to reduce the design spectrum based on calibration with time history analysis. The EVD includes mechanical damping of the devices and an additional 3% to account for contact damping (as discussed above). It is clear from Table 3 that the non-linear viscous dampers provide minimal damping capacity to the system.

While no trends can be derived from a single ground motion, some conclusions from a design procedure can be made. A significant reduction in displacement response could be achieved with relatively minimal increase to the capacity of the damper. Furthermore, the velocity limitation of the shake-table (due to the oil flow rate

within servovalves) prevented important ground motion characteristics from being replicated; namely, records characterised with large velocity pulses, typical of near-fault ground motions. If larger table velocities were possible, the capacity of the viscous dampers were increased and there was a larger dependency on velocity i.e. α>0.5, the benefits of such a system would be more evident. In fact, extensive numerical studies have confirmed the benefits of combining viscous and hysteretic dampers within self-centring systems (defined as advanced flag-shape systems) for protection against near-fault effects (Kam et al. [2007]). Recently, these numerical studies have been extended to multi-storey moment resisting frame structures where the interested reader is referred to the following companion paper; Kam et al. [2008].

Table 3. Performance assessment and measured response of the post-tensioned walls

	PT Wall HY_{0MS-4V}	PT Wall HY_{2MS-4V}	PT Wall HY_{2MS-0V}
Assessed EVD, ξ_{eq}	4.42%	10.27%	7.28%
Predicted displ, Δ_d	37.4mm (1.78% drift)	27.5mm (1.31% drift)	27.9mm (1.33% drift)
Measured max displ, Δ_{max}	35.0mm (1.67% drift)	27.6mm (1.32% drift)	28.7mm (1.37% drift)

5. CONCLUSIONS

Shake-table testing of post-tensioned rocking wall systems with viscous and hysteretic supplementary dampers demonstrated the dynamic response of the next generation, high-performance, self-centring systems. A series of free-vibration release tests allowed calibration of the EVD associated with contact damping. EVD equal to 3% of critical damping was found to represent the energy dissipation effectively, while tentative results indicated that this proportion of energy dissipation was independent on the amount of supplementary dissipation located within the wall. When subjected to recorded strong ground motion, the response of the wall was dependant on the type of mechanical dissipation adopted. A combination of viscous and hysteretic energy dissipation was found to be more effective at reducing displacements when compared to a viscous-only system with low energy dissipation capacity.

The experimental testing was used to assess a proposed displacement-based design procedure for the design of post-tensioned precast wall systems with viscous and hysteretic supplementary damping devices located at the rocking interface. The procedure extends on current Direct Displacement-Based Design philosophies (DDBD) and was found to be an efficient and reliable tool for design. The predicted displacements compared well with those measured during testing (maximum error of 6.6%). Work is ongoing in this area to further confirm and validate the EVD associated with contact damping and the extension of the proposed design procedure to MDOF systems. While the full benefits of viscous dampers could not be experimentally verified due to the velocity limitation of the shake-table, numerical studies are able to confirm their enhanced performance, especially for protection against near-fault ground motions.

6. APPENDIX: DESIGN EXAMPLE

To illustrate the design procedure in detail, the following example outlines the design of a full scale prototype structure based on the geometry in Figure 1 (a). This particular post-tensioned rocking wall is constructed with four non-linear dampers (two layers of viscous dampers, N_{vis}=2) each with a damping coefficient of C_{vd}=73.88kNs$^{\alpha}$/m$^{\alpha}$ and a non-linearity of α=0.153. In addition to the viscous dampers, a single layer (two dampers) of TCY mild-steel dampers with a diameter of d_{diss}=21mm and steel grade f_y=300MPa, is also installed (see HY_{2MS-4V} in Figure 4 (c) for more details).

Step 1: A target design drift of 1.31% (Δ_d=82.5mm lateral displacement) is chosen for design. The MDOF system is converted to an equivalent SDOF system with an effective height of h_e=6.3m and an effective mass of m_e=38.934tonne.

Step 2: The local damper coefficient C_{vd} is converted to a global damping coefficient C_{sys} using Figure 3 (a). Given an aspect ratio of A_r=3.5, α=0.153 the local-global damper ratio is estimated as β_{vd}=0.18 (followed by a refined calculation to equal β_{vd}=0.20). The global damping coefficient C_{sys} is computed; $C_{sys} = C_{vd}\beta_{vd}N_{vis} = 73.88kNs^{\alpha}/m^{\alpha} \cdot 0.20 \cdot 2 = 29.6kNs^{\alpha}/m^{\alpha}$.

Step 3: The system damping C_{sys} is normalised with respect to the critical damping C_c. i.e. $\Omega = C_{sys}/C_c$. The procedure is iterative as the effective period must be known in order to compute the critical damping of the system, $C_c = 2\omega_e m_e = 2 \cdot 6.96rad/s \cdot 38.934t = 541.8kNs/m$. The normalised damping coefficient is thus $\Omega = C_{sys}/C_c = 29.6/541.8 = 0.055$. The EVD associated with the viscous dampers ξ_{vis} is determined using Figure 3 (b) for far-field seismicity or (c) for near field seismicity. This graphical relationship can be expressed as a linear

equation $\xi_{vis} = a_0 + a_1\Omega$ where a_0 and a_1 are a function of the damper's non-linearity (α). For far-field seismicity and α=0.153, a_0=-0.013 and a_1=0.501, resulting in an EVD equal to ξ_{vis}=1.4%.

Step 4: The hysteretic proportion of EVD ξ_{hyst} is based on the ratio of the mild steel reinforcement and prestressed reinforcement moment ratio ($\lambda = M_{PT} / M_{ms}$, found by a moment-rotation section analysis). The system is assessed to have a ductility of μ=5.2 resulting in hysteretic EVD equal to ξ_{hyst}=5.8%.

Step 5: The total EVD ξ_{eq} is summed together accounting for an additional 3% attributed to contact damping. The total EVD is thus ξ_{eq}=1.4%+5.8%+3%=10.3%. The design displacement spectra is reduced by an amount equal to η=0.76 (Priestley et al. [2007]) resulting in an effective period of T_{eq}=0.90sec.

Step 6: The effective stiffness is computed and the base shear is calculated as $V_b = K_{eq}\Delta_{eq} = 1885kN/m \cdot 0.0825m = 155.5kN$. A final base shear reduction factor ϕ_{BL} is applied, based on numerical calibration. This reduction factor recognises the reduction in displacement response of a bilinear loading envelope when compared to a linear elastic loading envelope (with secant stiffness to the target displacement). The design base shear is thus equal to $V_b^* = \phi_{BL} V_b = 0.94 \cdot 155.5kN = 147kN$.

7. ACKNOWLEDGEMENTS

The authors acknowledge Dr Gabriella Castellano from *FIP Industriale* for the use of four viscous dampers and the assistance of Mr Masoud Maghaddasi during construction and testing. Financial support from the FRST projects; "Future Building Systems" and "Retrofit Solutions for New Zealand Buildings" is greatly appreciated.

REFERENCES

ACI:T1.2-03. (2007). ACI Manual of Concrete Practice-Special Hybrid Moment Frames Composed of Discretely Jointed Precast and Post-Tensioned Concrete Members.

fib. (2003). Seismic Design of Precast Concrete Building Structures, International Federation for Structural Concrete, Lausanne, Switzerland.

Kam, W. Y., Pampanin, S., Carr, A. and Palermo, A. (2007). "Advanced Flag-Shape Systems for High Seismic Performance Including Near-Fault Effects." NZSEE Conference, Palmerston North, New Zealand.

Kam, W. Y., Pampanin, S., Palermo, A. and Carr, A. (2008). "Implementation of advanced flag-shape (AFS) systems for moment-resisting frames structures." 14WCEE, Beijing, China.

Kurama, Y. C. (2002). "Hybrid post-tensioned precast concrete walls for use in seismic regions." *PCI Journal*, **47**:**5**, 36-59.

Kurama, Y. C., Sause, R., Lu, L. and Pessiki, S. (1999). "Seismic Behaviour and Design of Unbonded Post-Tensioned Precast Concrete Walls." *PCI Journal*, **44**:**3**, 72-89.

Kwan, W.-P. and Billington, S. L. (2003). "Unbonded posttensioned concrete bridge piers. I: Monotonic and cyclic analyses." *Journal of Bridge Engineering*, **8**:**2**, 92-101.

Marriott, D., Pampanin, S., Palermo, A. and Bull, D. (2008). "Dynamic Testing of Precast, Post-Tensioned Rocking Wall Systems with Alternative Dissipating Solutions." *Bulletin of the NZSEE*, **41**:**2**.

NZS1170.5. (2004). "Structural Design Actions, *Part 5: Earthquake actions*." Standards New Zealand, Wellington.

NZS3101. (2006). "Concrete Structures Standard: Part 1-The Design of Concrete Structures." Standards New Zealand, Wellington.

Palermo, A., Pampanin, S. and Calvi, G. M. (2005). "Concept and Development of Hybrid Solutions for Seismic Resistant Bridge Systems." *Journal of Earthquake Engineering. Vol. 9, no. 6, pp. 899-921. Nov. 2005.*

Pampanin, S. (2005). "Emerging solutions for high seismic performance of precast/prestressed concrete buildings." *Journal of Advanced Concrete Technology*, **3**:**2**, 207-223.

Priestley, M. J. N. (1999). "Preliminary results and conclusions from the PRESSS five-storey precast concrete test building." *PCI*, **44**:**6**, 42-67.

Priestley, M. J. N. (2003). Myths and Fallacies in Earthquake Engineering, Revisited.

Priestley, M. J. N., Calvi, G. M. and Kowalsky, M. J. (2007). Displacement-Based Seismic Design of Structures, IUSS PRESS, Pavia, Italy.

Solberg, K., Dhakal, R. P., Bradley, B., Mander, J. B. and Li, L. (2008). "Seismic performance of damage-protected beam-column joints." *ACI Structural Journal*, **105**:**2**.